Exclusive formation of alloy phases via anchoring technique - from bimetallic catalysts to electrocatalysis

CATALYSIS TODAY, Volume 306 (2018) 58-70.

Irina Borbáth, Dorottya Gubán, István Bakos, Zoltán Pászti, Gergely Gajdos, István E. Sajó, Ádám Vass, András Tompos

http://dx.doi.org/10.1016/j.cattod.2017.01.011

ISSN: 0920-5861; Source Type: Journal; Original language: English;
Document Type: Article; Publisher: Elsevier B.V.

Corresponding author: Irina Borbáth

Graphical abstract

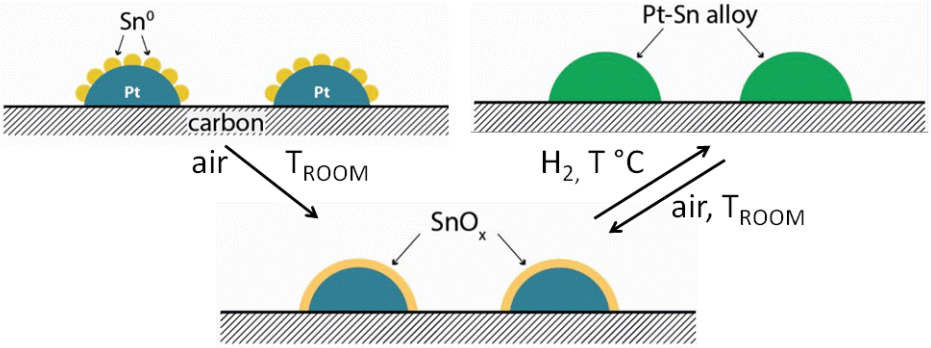

Exclusive formation of alloy phases via anchoring technique - from bimetallic catalysts to electrocatalysis

I. Borbáth[1*], D. Gubán[1], I. Bakos[1], Z. Pászti[1], G. Gajdos[1], I.E. Sajó[2], Á. Vass[1], A. Tompos[1]

[1]*Institute of Materials and Environmental Chemistry, Research Centre for Natural Sciences, Hungarian Academy of Sciences, H-1117 Budapest, Magyar tudósok körútja 2, Hungary*
[2]*University of Pécs, Szentágothai Research Centre, Pécs, H-7624, Ifjúság str. 20. Hungary*

Abstract:

Alloy-type Sn-Pt/C electrocatalysts with desired Pt/Sn= 3.0 ratio have been prepared using commercial 20 wt.% Pt/C (20Pt/C (Q: Quintech)) and home-made 20Pt/C (H) catalysts by means of Controlled Surface Reactions. According to *in situ* XPS and *in situ* XRD studies the exclusive incorporation of Sn onto the Pt sites was achieved resulting in exclusive formation of Pt-Sn alloy phase. No evidence of the presence of SnO_2 phase was found by means of the XRD and EDS analysis. According to *in situ* XPS studies pre-treatment of the air exposed catalyst in H_2 even at 170°C resulted in complete reduction of the ionic tin to Sn^0, suggesting alloy formation. After contact of Sn-Pt/C catalysts with air Sn tends to segregate to the surface, where it oxidizes to a certain extent. Reversible interconversion of PtSn ↔ Sn^{4+} + Pt in the presence of O_2 and H_2 was convincingly demonstrated by *in situ* XPS and *in situ* XRD studies.
The electrocatalytic performance of the alloy catalysts was tested in CO oxidation and oxygen reduction reaction (ORR). Only minor changes of the surface composition of Sn-20Pt/C electrocatalysts were observed after 20 polarization cycles. Better performance in the CO electrooxidation for our Sn-Pt/C catalysts compared to the state-of-art CO tolerant PtRu/C benchmark was demonstrated. Optimal surface composition of the Sn-20Pt/C (H) catalysts results in increased activity in the ORR compared to the Sn-20Pt/C (Q) and both parent 20Pt/C catalysts.

Keywords: PtSn/C electrocatalysts, Controlled surface reactions, Pt_3Sn, Anode catalyst, Oxygen reduction reaction, CO electrooxidation

1. Introduction

1.1 Sn-Pt/C electrocatalysts: requirements and preparation methods

Polymer electrolyte membrane fuel cells (PEMFC) are expected to be one of the key devices to solve energy and environmental problems [1]. For the wide-range implementation of PEMFC, it is most essential to produce low-cost durable units. A significant part of the price belongs to the electrocatalysts, which contain high loadings of Pt. Key requirements for the implementation of fuel cells are: (i) reducing the amount of Pt; (ii) increasing of the metal dispersion; (iii) stability during long time application; (iv) high CO tolerance of the anode electrocatalysts, and (v) high activity and selectivity of the cathode electrocatalysts in the oxygen reduction reaction (ORR). One of the important approaches is to use co-catalysts in

* Corresponding author, Tel.: +36 1 382 6916, email: borbath.irina@ttk.mta.hu, address: H-1519 Budapest, P.O.Box 286, Hungary (Irina Borbáth)

combination with platinum. A variety of transition metals have been used as co-catalysts such as Ru, Mo, Ni or Sn [2-4]. Amongst those, Sn-modified Pt/C supported electrocatalysts are recognized as the most active electrodes for the CO, methanol and ethanol oxidation reactions [5,6] and the ORR [7].

Most synthetic routes of Sn-Pt/C electrocatalysts lead to solids with a wide range of phases such as Pt, either reduced or as oxide, Sn oxides and Pt-Sn alloys or solid solutions with different stoichiometry [8]. The promoting effect of different forms of Sn on the activity of Pt-based catalysts has been comprehensively analyzed by Antolini and Gonzalez [9]. In analyzing various reports, it seems that production of Pt_3Sn as a pure and exclusive phase rarely occurs and its amount strongly depends on the synthetic procedure [9,10], even if this phase is associated with the best electrocatalytic properties [5]. Carbon-supported Pt-based alloy nanoparticles can be prepared by following methods: impregnation [11], water-in-oil microemulsion methods [12], the well-known "Bönnemann" method [13], the polyol synthesis [14], the borohydride [15] and formic acid [16] reduction methods, the polymeric precursor method [17]. Controlled formation of Pt-Sn alloy nanoparticles with cubic and hexagonal structure has been achieved by the "heating up" method [18].

1.2 Surface organometallic chemistry of tetraalkyl tin

Exclusive formation of supported Sn-Pt alloy phases with different Sn/Pt ratios can also be achieved by using Controlled Surface Reactions (CSRs) [19]. The surface chemistry of the tin anchoring reaction can be written as follows:

$$PtH_{ads} + Sn(C_2H_5)_4 \rightarrow Pt\text{-}Sn(C_2H_5)_{(4-x)} + x\ C_2H_6 \quad (1)$$

$$Pt\text{-}\ Sn(C_2H_5)_{(4-x)} + (4-x)/2\ H_2 \rightarrow Pt\text{-}Sn + (4-x)\ C_2H_6 \quad (2)$$

During the tin anchoring (step I) the organometallic precursors decompose only partly on the metal particle and surface organometallic species stabilized on the metal surface are formed (see Eq. (1)). Decomposition of these surface species (step II) can be done in hydrogen or oxygen atmosphere. Upon decomposition in hydrogen (see Eq. (2)) the net result is the exclusive formation of Pt-Sn alloy-type surface species as evidenced by Mössbauer spectroscopy [20]. Whereas decomposition in oxygen results in the formation of Lewis-acid type sites consisting of finely dispersed SnO_x surface species anchored onto the active metal creating the "metal ion-metal nano-cluster" ensemble sites [21]. The formation of the above species was evidenced by Mössbauer [20] and FTIR spectroscopy [22].

In our previous studies the modes and ways to increase the amount of tin introduced directly onto the parent metal has also been established. Based on CSRs a new method was developed for the preparation of different types of supported bimetallic (E_x-M_y, where E= Sn, Ge; M= Pt, Pd, Rh, Ru) catalysts with exclusive formation of metal-metal interaction even at high E/M ratios [23-26].

It has to be emphasized that the exclusive formation of tin-metal interaction requires special control to avoid the reactions with the involvement of surface OH groups [22,27-28]. Organometallic species anchored onto the support, formed upon using conditions favoring this side reaction, can be decomposed either in hydrogen or oxygen atmosphere with formation of SnO_x species grafted onto the support. It is necessary to mention that low-valent cations of an oxophilic metal grafted onto a support has an ability to stabilize small (1-2 nm) noble metal nanoparticles (e.g. gold [28]).

Catalysts prepared in this way showed unique properties in low temperature CO oxidation [29], selective hydrogenation of organic compounds (unsaturated aldehydes, citral, benzonitrile [23,24,30,31]), *n*-butane dehydrogenation [27], hydrogen-assisted 1,2-dichloroethane dechlorination [32] and naphtha reforming [33]. Our new results demonstrate [5,34,35] that upon using CSRs Sn-modified 40 wt.% Pt/C electrocatalysts highly active in both the electrooxidation of CO and C_1-C_2 alcohols can be prepared.

In this contribution we report the peculiarities of commercial and home-made 20 wt.% Pt/C catalysts modification with Sn by CSRs with the aim to synthesize electrocatalysts with the desired nominal ratio Pt/Sn= 3 and homogeneous tin distribution over the Pt nanoparticles. The performance of these catalysts is also evaluated in both the CO electrooxidation reaction and the ORR.

2. Material and methods

2.1 Materials

The organometallic compound (tetraethyltin, $Sn(C_2H_5)_4$), platinum precursor ($H_2PtCl_6 \cdot 6H_2O$) and solvents (*n*-decane and *n*-hexane) were used as received (Sigma-Aldrich). Ethylene glycol (EG), $NaBH_4$, absolute ethanol, isopropanol, H_2SO_4 and HCl were purchased from Molar Chemicals. Abbreviations are listed in the Supplementary material.

2.2 Synthesis of home-made 20 wt.% Pt/C electrocatalyst

The home-made 20 wt.% Pt/C catalyst (20Pt/(H)) was prepared by $NaBH_4$-assisted EG reduction method using active carbon as a support (CABOT, Black Pearls 2000, 1475 $m^2\ g^{-1}$) and ethanol as a solvent. It should be noted that in Ref. [36] EG was used as a solvent.

H_2PtCl_6 (166 mg) was solved in 25 ml absolute ethanol and 200 mg of the support material was suspended in the solution. Hereupon a solution prepared by the reaction of $NaBH_4$ (590 mg) and EG (7.4 ml) was added dropwise to the suspension at 65 °C with stirring. After 3 h of stirring at 65 °C, 15 ml 0.5 M HCl was added to the suspension and stirred for an additional 2.5 h at room temperature (RT) to deposit the Pt particles onto the support material. The material was washed with water (18.2 MΩ) by centrifugation and dried at 80 °C overnight.

2.3 Synthesis of Sn modified Pt/C catalysts

Commercial 20 wt.% Pt (Quintech, C-20-Pt, Pt= 20 wt.% on Vulcan support; denoted hereafter as 20Pt/C (Q)) and 20Pt/(H) catalysts were modified with $Sn(C_2H_5)_4$ by CSRs. Tin anchoring (step I) was performed in a 40 ml stainless steel autoclave at 170°C using P_{H2}= 5 bar and three or five consecutive tin anchoring periods. Detailed description of the synthesis procedure can be found in Ref. [34].

Pt/C catalyst was suspended in *n*-decane. The autoclave was purged with hydrogen for 10 min and then the hydrogen pressure was set up to 5 bars. The reactor was immersed in an oil bath and heated up to 170°C, then the tin anchoring step I was started by an addition of the appropriate amount of $Sn(C_2H_5)_4$ solution in decane. For this purpose the calculated amount of tetraethyltin (needed for the preparation of Sn-Pt/C catalysts with desired Pt/Sn= 3 ratio) was divided into three or five equal portions and introduced into the reactor after equal periods of time. Preparation details are listed in Table 1. After the modification procedure, the catalyst was separated by centrifugation and carefully washed twice with decane and tree times with hexane. The catalyst was dried in air at 60°C overnight.

Decomposition in hydrogen (step II) was accomplished by Temperature Programmed Reduction (TPR) technique (heating rate= 5°C min^{-1}, hydrogen flow rate= 30 ml min^{-1}). The final temperature (T_{red}) applied was 250 or 350°C. Catalysts were kept at final temperature for 2 h then the furnace was cooled down in flowing H_2 to RT. Finally, the atmosphere was changed to N_2.

2.3 Physical characterization

In situ X-Ray Diffraction (XRD) experiments were carried out by a Philips model PW 3710 based PW 1050 Bragg-Brentano parafocusing goniometer in a heated sample holder Anton Paar HTK 1200 using CuK_α radiation (λ= 0.15418 nm) operating at 40 kV and 35 mA,

graphite monochromator and proportional counter. Silicon powder (NIST SRM 640) was used as an internal standard and the scans were evaluated with profile fitting methods. The cell parameters of the crystalline phases were determined from the fitted d-values.

About 50 mg catalyst sample was loaded into the cell and a powder XRD measurement was carried out in the 2 theta range of 10 to 90 degrees at a scanning speed of 0.02° s^{-1}. Then after purging with N_2 for 15 min the sample was heated up to 200°C with a rate of 5°C min^{-1} in H_2 flow and kept at constant temperature for 2 h, then another XRD pattern was recorded as described earlier. The same procedure was repeated at 250, 300 and 350°C, respectively. After the measurements the sample was cooled down to RT in H_2 and XRD pattern was recorded. Then after purging with N_2 15 min the sample was exposed to air for 24 h and then XRD measurements were carried out again.

Transmission Electron Microscopy (TEM) studies of the samples were made by use of a FEI Morgagni 268D type transmission electron microscope (accelerating voltage: 100 kV, W-filament). The fresh samples were prepared by grinding and dispersing of the resulted powder in ethanol using an ultrasonic bath. A volume of the obtained suspension was pipetted onto a carbon coated copper grid. The average diameter was calculated by measuring the diameters of no less than 600-700 randomly selected metal particles from the non-aggregated areas in at least tree micrographs of each sample.

Energy Dispersive X-ray Spectrometry (EDS) analysis was performed with an INCA (Oxford Instruments Ltd.) detector and the INCAEnergy software package. EDS analysis of individual particles was possible by using ZEISS EVO 40XVP Scanning Electron Microscope (accelerating voltage: 20kV, W-filament).

X-ray photoelectron spectroscopy (XPS) measurements were carried out using an electron spectrometer manufactured by OMICRON Nanotechnology GmbH (Germany). The photoelectrons were excited by MgKα (1253.6 eV) radiation. Spectra were recorded in the Constant Analyser Energy mode of the EA125 energy analyser with 30 eV pass energy resulting in a spectral resolution of 1 eV. A custom-built high pressure chamber attached to the electron spectrometer allows to simulate the annealing steps of the catalyst preparation and activation under well controlled conditions, thus bonding and compositional changes induced by these steps can be analyzed without the need for air exposure. Samples in the form of fine powder were suspended in hexane. Drops of this suspension were placed on standard OMICRON sample plates; after evaporation of hexane catalyst coatings with sufficient adhesion and electric conductivity were obtained. Samples were first analyzed in the "as received" state. The next measurements were made after reduction in the high pressure chamber in 300 mbar H_2 at different temperatures for 2 h (see details in Tables S1, S2 and S3 in the Supplementary material); during these experiments air exposure was avoided (*in situ* experiments).

Binding energies were referenced to the main component of the C 1s spectrum of the support (graphite at 284.4 eV binding energy). Data were processed using the CasaXPS software package [37] by fitting the spectra with Gaussian-Lorentzian product peaks after removing a Shirley or linear background. Nominal surface compositions were calculated using the XPS MultiQuant software package [38,39], with the assumption of homogeneous depth distribution for all components. Chemical states were identified by XPS databases [40,41].

2.4 Electrochemical characterization

The Sn-Pt/C electrocatalysts were investigated by means of cyclic voltammetry (CV) and adsorbed CO (CO_{ad}) stripping technique in a conventional three-electrode electrochemical glass cell using a Biologic SP150 potentiostat and the EC-LAB software package. The working electrode was prepared by supporting the electrocatalysts on a glassy carbon (GC)

electrode (d = 0.3 cm, geometric surface area A = 0.0707 cm^2). Before each test the glassy carbon disc was polished with 0.05 μm alumina to obtain a mirror finish, followed by ultrasonic cleaning in water (18.2 MΩ cm), isopropanol and again water to remove any traces of organic impurities. The samples under study were deposited onto the GC by means of a catalyst ink.

2 mg of the electrocatalyst, 0.4 ml of isopropanol, 1.592 ml of water (18.2 MΩ cm) and 8 μl of Nafion solution (DuPont™ Nafion® PFSA Polymer Dispersions DE 520) were dispersed in an ultrasonic bath for 45 min, resulting in a homogeneous ink. After ultrasonic dispersion an 3.6 μl aliquot has been dropped over the GC surface and dried in air leading to a homogeneous coating. Pt was used as counter electrode. The reference electrode was reversible hydrogen electrode (RHE). The applied electrolyte was 0.5 M H_2SO_4. Prior to the measurements, the electrode was activated by potential cycling for 10 times in the range 50 and 1000 mV (vs. RHE) at a scan rate of 100 mV s^{-1}. After the activation procedure, CV measurements were done in the potential range of 50-1000 mV at a scan rate of 10 mV s^{-1}.

The amount of CO_{ad} has been measured by CO stripping voltammetry in 0.5 M H_2SO_4. Gaseous CO was fed into the cell for 30 min while maintaining the electrode potential constant at 50 mV. After CO removal from the solution (Ar purge for 30 min), the working electrode was subjected to a CV measurement at a scan rate of 10 mV s^{-1} between 50 and 1000 mV. The amount of adsorbed CO was evaluated by integration of the CO stripping peak. For comparison PtRu/C electrocatalyst (Quintech C-20-/10-Pt/Ru, Pt= 20 wt%, Ru= 10 wt% on Vulcan) was also studied in the CO_{ads} stripping.

The electrochemically active Pt surface area (ECSA) values were calculated from the charge associated with a CO monolayer adsorbed onto the Pt nanoparticles ($ECSA_{CO}$) and from the hydrogen adsorption/desorption region ($ECSA_H$) observed on the CVs. The $ECSA_{CO}$ related to unit weight of Pt was calculated assuming a monolayer of linearly adsorbed CO and the charge necessary for its oxidation considering 420 μC cm^{-2}. For $ECSA_H$ calculations the charge of 210 μC cm^{-2} is widely accepted and used [42].

Catalytic activity of the catalyst samples was tested in the ORR by rotating disk electrode (RDE) technique in O_2 saturated 0.5 M H_2SO_4 solution at ambient temperature and pressure. GC electrode of 5 mm diameter (geometric surface area: 0.196 cm^2) was used in these measurements. 10 μl catalyst ink was dropped on the freshly polished GC electrode which resulted in about 10 μg cm^{-2} Pt loading. Polarization curves were recorded by sweeping the potential between 300 and 1000 mV with 10 mV s^{-1} sweep rate, rotating the electrode at 225, 400, 625, 900 and 1225 rpm. Data were obtained from the negative scans. In order to characterize the surface state of the catalysts, before and after the RDE measurements 10 CVs between 50 and 1000 mV potential limits in Ar saturated electrolyte were also measured.

3. Results and discussion

3.1 Modification of commercial Pt/C catalyst with tetraethyltin

Experimental results related to tin anchoring onto the 20Pt/C (Q) catalyst are summarized in Table 1. We reported earlier [34] that in the preparation of the catalysts with high tin content the application of the consecutive anchoring reactions using lower initial $Sn(C_2H_5)_4$ concentration can be very promising. It has been demonstrated [43] that the use of extremely high tetraethyltin concentration should be avoided, since it can lead to the concentration gradient of the anchored modifier. The use of consecutive reaction steps avoids any inhomogeneity of the modifier over the metallic particles.

Table 1. Influence of the preparation conditions of the Sn-20Pt/C catalysts on the particle size and electrochemical performance (for comparison results obtained on two parent 20Pt/C catalysts are also included (Q: Quintech and H: home-made)).

Samples [a]	V_{SnEt4}, [b] µl	Number of periods	T_{red}, °C	TEM, nm	$E_{CO,onset}$, mV	$ECSA_{CO}$, [d] m^2/g_{Pt}
20Pt/C (Q)	-	-	-	2.6±0.8	625	60.7 ± 3.8
Sn-20Pt/C-III (Q)	760	3	without TPR [c]	2.8±1.2	255	45.0 ± 1.1
Sn-20Pt/C-III (Q)	760	3	250 (2 h)	3.2±1.5	215	45.6 ± 6.3
Sn-20Pt/C-III (Q)	760	3	350 (2 h)	5.6±4.5	300	46.1 ± 1.6
Sn-20Pt/C-V (Q)	456	5	without TPR [c]	n.m.	250	44.4 ± 0.7
20Pt/C (H)	-	-	-	2.0±1.1	615	77.0 ± 7.7
Sn-20Pt/C-V (H)	456	5	without TPR [b]	n.m.	205	63.3 ± 1.2
Sn-20Pt/C-V (H)	456	5	250	2.4±1.1	205	56.7 ± 1.2
Sn-20Pt/C-V (H)	456	5	350	3.4±1.4	210	62.6 ± 0.8

Amount of the 20Pt/C catalyst: 0.2 g; solvent: *n*-decane (V_{C10H22}= 10 ml); concentration of $SnEt_4$ solution: $[SnEt_4]_0$= 0.031 M; total amount of tin introduced during tin anchoring step I: $SnEt_4$= 0.07 mmol.

[a] Roman number used in denomination of the samples indicates the number of tin anchoring periods (three or five);

[b] Amount of *n*-decane solution of $SnEt_4$ added in one tin anchoring period;

[c] Without TPR: catalyst used after modification and drying procedure, without high-temperature treatment in H_2;

[d] $ECSA_{CO}$ values were calculated from the CO-stripping measurements;

n.m., the sample was not measured.

It is necessary to mention that upon modification of 20Pt/C (Q) catalyst five consecutive tin anchoring periods were applied only for the purpose of comparison with results obtained on our Sn-modified home-made 20Pt/C catalysts. 20Pt/C (H) catalyst was prepared using Black Pearls 2000 as active carbon support, which has high amount of surface functional groups and large surface area. These properties might favor the side reaction, which results in tin-support interaction. The probability of this reaction can be decreased using both lower concentration of $Sn(C_2H_5)_4$ and increased number of tin anchoring periods. Such precautions are not necessary in case of relatively inert Vulcan with surface area of about 254 $m^2\ g^{-1}$. The properties and behavior of samples, which were obtained using three and five consecutive tin anchoring periods and studied without any high-temperature treatment (HTT), were similar (see Table 1).

Microstructure of the Sn-20Pt/C (Q) electrocatalysts

In the present study in order to increase the content of the desired fcc Pt_3Sn phase and to minimize the sintering of the metal nanoparticles an attempt was done to optimize the final temperature of the H_2 treatment (T_{red}) applied in TPR experiments (step II).

The influence of the T_{red} on the type of Sn-Pt alloys was demonstrated in Ref. [44]. It has been shown that reduction at 400°C of unsupported Pt-Sn powder with a nominal Pt/Sn= 3 atomic ratio was necessary to achieve the exclusive formation of the Pt_3Sn alloy phase. However, it has also been known that catalysts supported on functionalized carbon could not tolerate HTT, due to the instability of surface oxygen groups of the support, which act as primary anchoring centers for metal precursors, facilitating the high dispersion of the metal phase [45].

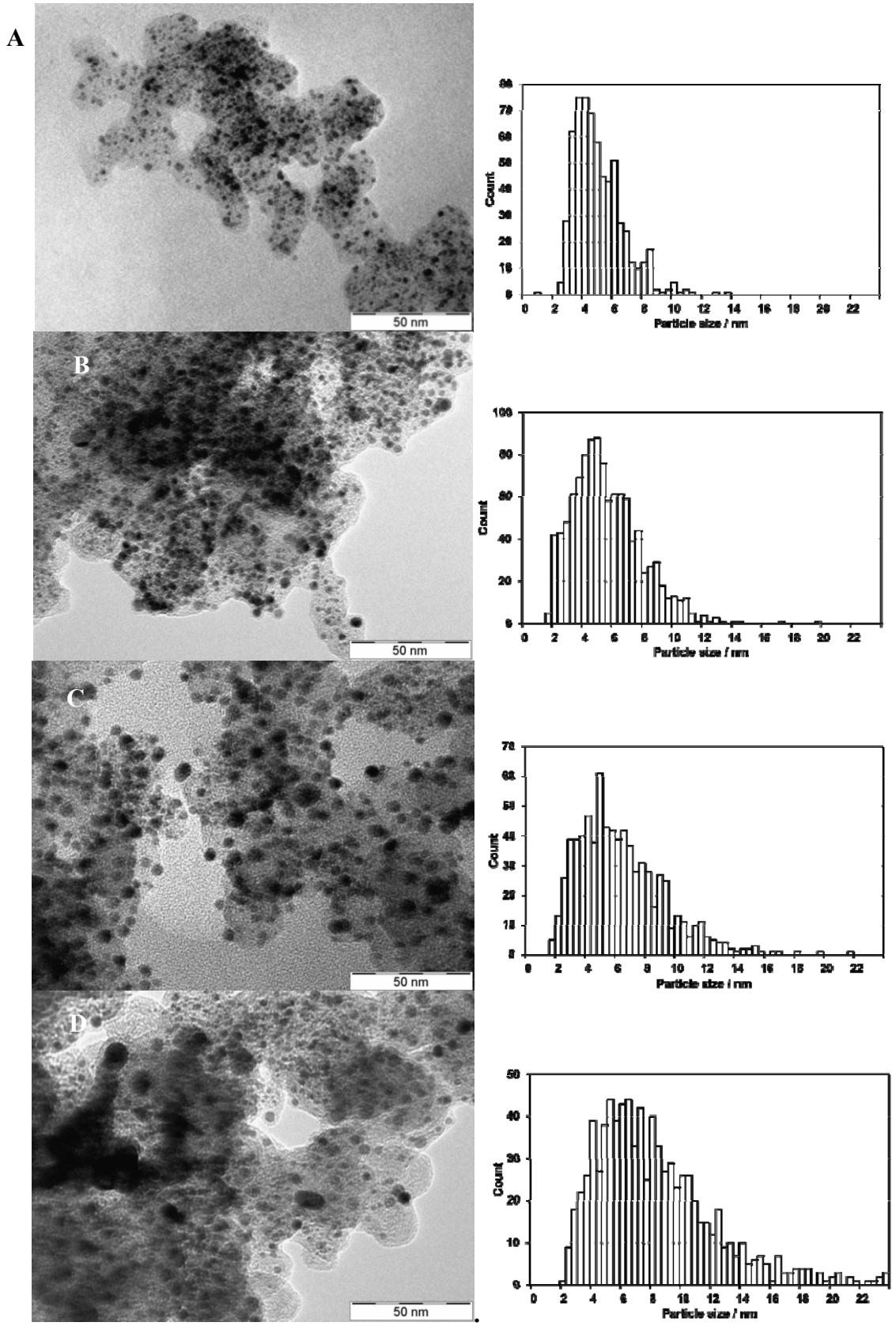

Fig. 1. TEM images and histograms of particle size distribution for the 20Pt/C (Q) catalyst (A) and the Sn-20Pt/C-III (Q) samples studied after tin anchoring step I without any HTT (B); after HTT in H_2 at T_{red}= 250 °C (C) and T_{red}= 350 °C (D).

It has been reported [46] that the stronger acid groups (e.g. carboxylic, anhydride groups) decomposed at 273°C, whereas for the decomposition of the weaker acid sites (e.g. lactone, phenol, carbonyl groups) higher temperatures should be applied (407°C).

Based on these observations the samples were studied after tin anchoring step I (without TPR) and after TPR experiments using different T_{red} (T_{red}= 250 and 350°C, details see in Table 1).

The size of Pt in parent Pt/C (Q) catalyst and the bimetallic nanoparticles of the Sn-20Pt/C-III (Q) samples after different HTT were checked by TEM (see Table 1 and Fig. 1A-D). TEM micrographs show the presence of spherical metallic particles supported on carbon. The mean diameter derived from the size distribution for the 20Pt/C (Q) is 2.6±0.8 nm.

It is known that incorporation of tin results in an increase of the size of the bimetallic particles. For the Sn-20Pt/C-III (Q) sample prepared using three consecutive tin anchoring periods and studied without TPR (see Fig. 1B) only negligible increase of the mean particle sizes was observed (2.8±1.2 nm). The influence of the treatment at 250°C and 350°C in H_2 atmosphere on the particle size was demonstrated in Figs. 1C and 1D. Applying of lower reduction temperature (250°C) results in still rather small particles with narrow size distribution (3.2±1.5 nm). The following increase of the T_{red} up to 350°C resulted in certain increase of the average crystallite size (5.6±4.5 nm).

XPS analysis of the Sn-Pt/C (Q) electrocatalysts

It is necessary to mention that after modification of a Pt/C catalyst in hydrogen atmosphere at T= 170°C and P_{H2}= 5 bar, all tin is in the Sn^0 state, existing probably in the form of adatoms and /or in a form of Sn-Pt alloy phases [34]. However, contact of the samples with air during washing, drying and storage results in oxidation of some part of tin (or even platinum) in Sn-Pt/C catalysts. The degree of oxidation strongly depends on both (i) the size of bimetallic particles and (ii) the temperature and prolongation of the contact with air. It can be proposed that highly dispersed nanoparticles (about 2-4 nm) can be oxidized to higher extent than bigger Sn-Pt particles. In order to clarify the nature of this unavoidable oxidation, not only the "as received" (i.e., air exposed) state of the catalysts was analyzed by photoelectron spectroscopy, but efforts were made to explore the consequences of high temperature reductive treatments with the exclusion of air via *in situ* experiments using the high pressure chamber of the electron spectrometer,

In photoelectron spectra of tin compounds usually two features are used for assessing the chemical state of tin: the binding energy of the Sn $3d_{5/2}$ core level and the kinetic energy of the Sn $M_4N_{45}N_{45}$ X-ray excited Auger transition. According to reference measurements on SnO_2 supported by carbon, the Sn $3d_{5/2}$ peak of fully oxidized tin is relatively broad and symmetric with a binding energy of 487.1 eV (see Fig. 2A), while the Sn $M_4N_{45}N_{45}$ Auger transition is a well-defined, narrow peak at 431.6 eV (see Fig. 2B). The so called modified Auger parameter, the sum of the Sn $3d_{5/2}$ binding energy and the Sn $M_4N_{45}N_{45}$ Auger kinetic energy is a sensitive probe for the ionic state of Sn; its value of 918.7 eV corresponds very well to that reported for SnO_2. In case of bulk metallic tin, the Sn $3d_{5/2}$ binding energy of 485.0 eV and the $M_4N_{45}N_{45}$ Auger kinetic energy of 437.4 eV results in an Auger parameter value of 922.4 eV [40,41].

In Fig. 2 XPS spectra of the Sn 3d region for the Sn-20Pt/C-III (Q) and Sn-20Pt/C-V (Q) samples are presented after different treatments, along with the corresponding Sn $M_4N_{45}N_{45}$ Auger spectra. Further results of the XPS analysis of these samples are summarized in Tables S1 and S2 in the Supporting material.

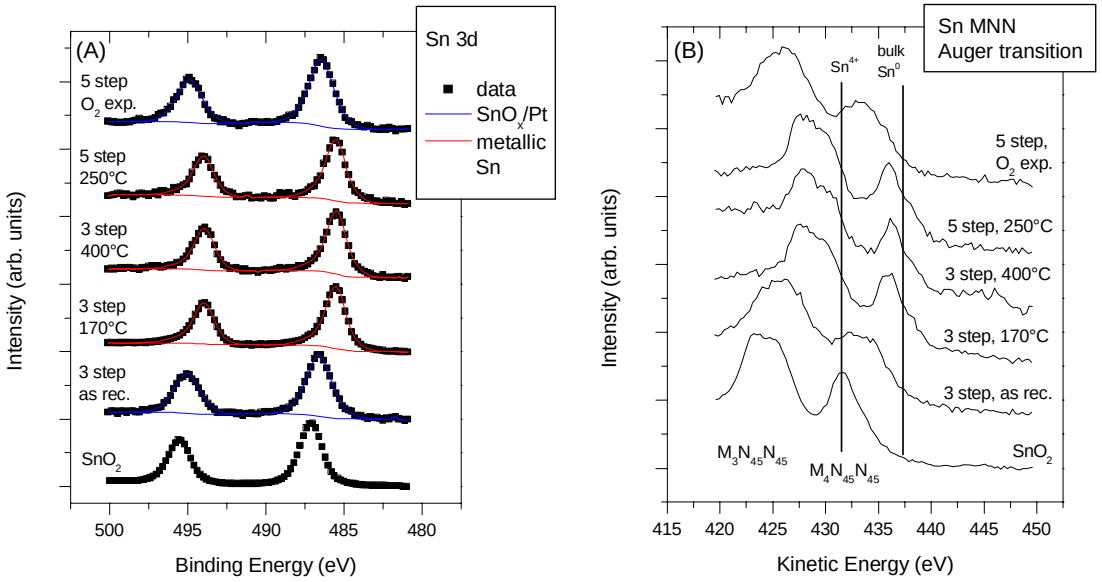

Fig. 2. (A): Sn 3d core level and (B): Sn MNN Auger spectra of the Quintech 20Pt/C catalysts modified by tin (Sn-20Pt/C-III (Q) and Sn-20Pt/C-V (Q)) in the as synthesized state and after reduction in 300 mbar H_2 for 2 hours at the indicated temperatures. The number of the consecutive tin anchoring steps is also indicated. The uppermost spectrum was measured on the Sn-20Pt/C-V (Q) sample reduced at 250°C, followed by oxidation in 100 mbar O_2 for 15 min at 250°C. For reference, spectra collected on SnO_2 are also presented. The Sn 3d spectra are corrected for the $MgK\alpha_{3,4}$ satellites. In (B), vertical lines indicate the position of the $M_4N_{45}N_{45}$ peak for SnO_2 and bulk metallic Sn.

In the *as received* Sn-20Pt/C-III (Q) sample a relatively broad but symmetric Sn $3d_{5/2}$ peak was found at 486.6 eV (see Fig. 2A). The Sn $M_4N_{45}N_{45}$ Auger transition appears at the kinetic energy of 432.4 eV, resulting in an Auger parameter value of 919.0 eV (see Fig. 2B). Although the Auger parameter is relatively close to that of SnO_2, the Auger line is rather broad and featureless, suggesting the presence of more than one ionic state for tin. One possibility is that tin deposited exclusively onto Pt during the CSRs becomes only incompletely oxidized upon air exposure, resulting in a mixture of Sn^{2+} and Sn^{4+} species. As the Sn $3d_{5/2}$ binding energy for SnO and SnO_2 seems to be almost identical and the difference between their Auger kinetic energies is also limited [47], our data are not in contradiction with this assumption. Indeed, the literature also tends to assign Sn $3d_{5/2}$ signals around 486.0-486.5 eV to Sn^{2+}-like species, rather than to Sn^{4+} [48-50]. Nevertheless, the little difference between the Auger parameters of the SnO_2 reference and the *as received* Sn-20Pt/C-III (Q) sample still may indicate that the dominant tin species is Sn^{4+}, with spectral features shifted because of electron transfer from the Pt. Pt itself is mostly metallic with a Pt $4f_{7/2}$ binding energy of 71.2 eV; a very small contribution (roughly 7% of the total Pt amount) arises around 72.5 eV due to oxidized platinum species (Pt^{2+}, [51,52]).

The metal content expressed in weight percent is not very far from the expected values: Pt= 22 wt.%, Sn= 10 wt.%. The Pt/Sn atomic ratio is around 1.4. The relatively high apparent Sn content suggests segregation of oxidized Sn on the Pt particles.

For comparison the Sn-20Pt/C-V (Q) catalyst obtained using five consecutive tin anchoring periods was also studied. The chemical states in this sample are essentially identical to those found in the Sn-20Pt/C-III (Q) catalyst. According to the detailed results

summarized in Table S2 (Supporting material), the metal content expressed in weight percent is Pt= 22 wt.%, Sn= 7 wt.%; the Pt/Sn atomic ratio is around 1.9. These values still indicate more Sn than the intended Pt/Sn ratio of 3, confirming the segregated nature of tin. Interestingly, the use of five tin anchoring steps during the preparation procedure seems to result in smaller tin excess than the three tin anchoring steps route.

The reductive treatment of the Sn-20Pt/C-III (Q) sample at 170°C for 2 h in 300 mbar H_2 resulted in essentially complete reduction of tin. The Sn $3d_{5/2}$ binding energy of 485.5 eV is somewhat high for bulk metallic Sn (485.0 eV or below). Nevertheless, metallic Sn binding energies shifted towards higher values by a few tenths of an eV are usually reported for Pt-Sn alloys [48,50,53]. Similarly, the Sn $M_4N_{45}N_{45}$ Auger kinetic energy of 436.0 eV giving an Auger parameter of 921.5 eV also suggests a metallic environment, although in bulk metallic tin the Sn $M_4N_{45}N_{45}$ Auger peak is at higher kinetic energy (437.4 eV). Thus the somewhat high $3d_{5/2}$ binding energy and low MNN kinetic energy point to alloy formation. Platinum is fully metallic after this reduction step. The reduction behavior is not influenced by the number of consecutive Sn deposition steps, as essentially the same chemical state results were obtained for the Sn-20Pt/C-V (Q) sample reduced at 200°C.

Elevating the reduction temperature to 250°C, 350°C and 400°C resulted in practically no change in the chemical states of the sample or in the composition. The Pt/Sn atomic ratio for Sn-20Pt/C-III (Q) is around 2.1, indicating that a portion of tin is still segregated on the surface of the metallic particles. Indeed, according to the literature, in Pt-Sn alloys there is a clear tendency for surface segregation of tin [53,54]; the nature of the segregation seems to be also related to the Pt particle size [55]. On the other hand, for the Sn-20Pt/C-V (Q) catalyst reduced at 250°C, the Pt/Sn atomic ratio is around 2.7, closer to the expected value of 3.0.

In order to get information about the oxidation behavior of the Sn-20Pt/C-V (Q) sample, after the reduction step at 250°C it was exposed to 100 mbar O_2 at 250°C for 15 min. The oxidation essentially restored the *as received* situation (see also Table S2 of the Supporting material). Pt remained predominantly metallic with a slight (around 10 %) ionic (Pt^{2+}) contribution. At the same time, metallic tin completely disappeared; the Sn $3d_{5/2}$ binding energy at 486.5 eV indicates the formation of the oxide phase strongly associated with Pt (see Figure 2A). Neither in the Sn 3d spectrum nor in the Sn $M_4N_{45}N_{45}$ Auger spectrum is metallic Sn evident, which suggests a substantial phase separation. The Sn $M_4N_{45}N_{45}$ Auger line is at a slightly higher kinetic energy as in the case of the *as received* Sn-20Pt/C-V (Q) sample (at 433.1 eV, instead of 432.6 eV, giving an Auger parameter value of 919.6 eV), which may suggest a more Sn^{2+}-like character for the oxidized situation.

This oxidation experiment indicates the reversible nature of the phase separation in Pt-Sn nanoparticles. Under oxidative conditions Sn tends to segregate to the surface, where it oxidizes to a certain extent. Under reductive conditions this tin oxide completely reduces to the metallic state and a significant part of the tin diffuses into the interior of the particles, forming a Pt-Sn alloy or intermetallic compound. Nevertheless, the surface of the reduced Pt-Sn particles still contains some excess (metallic) Sn. The segregated nature of the oxidized tin is also reflected by the compositional data obtained on the oxidized Sn-20Pt/C-V (Q) sample: the metal content expressed in weight percent is Pt= 20 wt.%, Sn= 7 wt.%. The Pt/Sn atomic ratio is 1.8, close to the value observed in the *as received* state.

The described dynamic behavior of the Pt-Sn catalyst induced by the oxidative or reductive nature of the environment is in good agreement with literature results obtained during ambient pressure XPS investigation [48] or diffuse reflectance infrared studies [56] of CO oxidation over colloidal Pt-Sn model systems. Even CO in H_2 seems to influence the surface composition of these bimetallic catalysts [57].

3.2 Modification of home-made 20 wt.% Pt/C catalysts with tetraethyltin

Considering the large number of the surface functional groups of the Black Pearls 2000 carbon support upon modification of the 20Pt/C (H) catalyst with $Sn(C_2H_5)_4$ five tin anchoring steps were used (see Table 1).

Microstructure of the Sn-modified home-made 20Pt/C electrocatalysts

TEM images and histograms displaying particle size distribution of the 20Pt/C (H) and Sn-modified catalysts are depicted in Fig. 3. The uniform distribution of spherical Pt particles for the 20Pt/C (H) with mean diameter of (2.0 ± 1.1) nm was verified via TEM imaging.

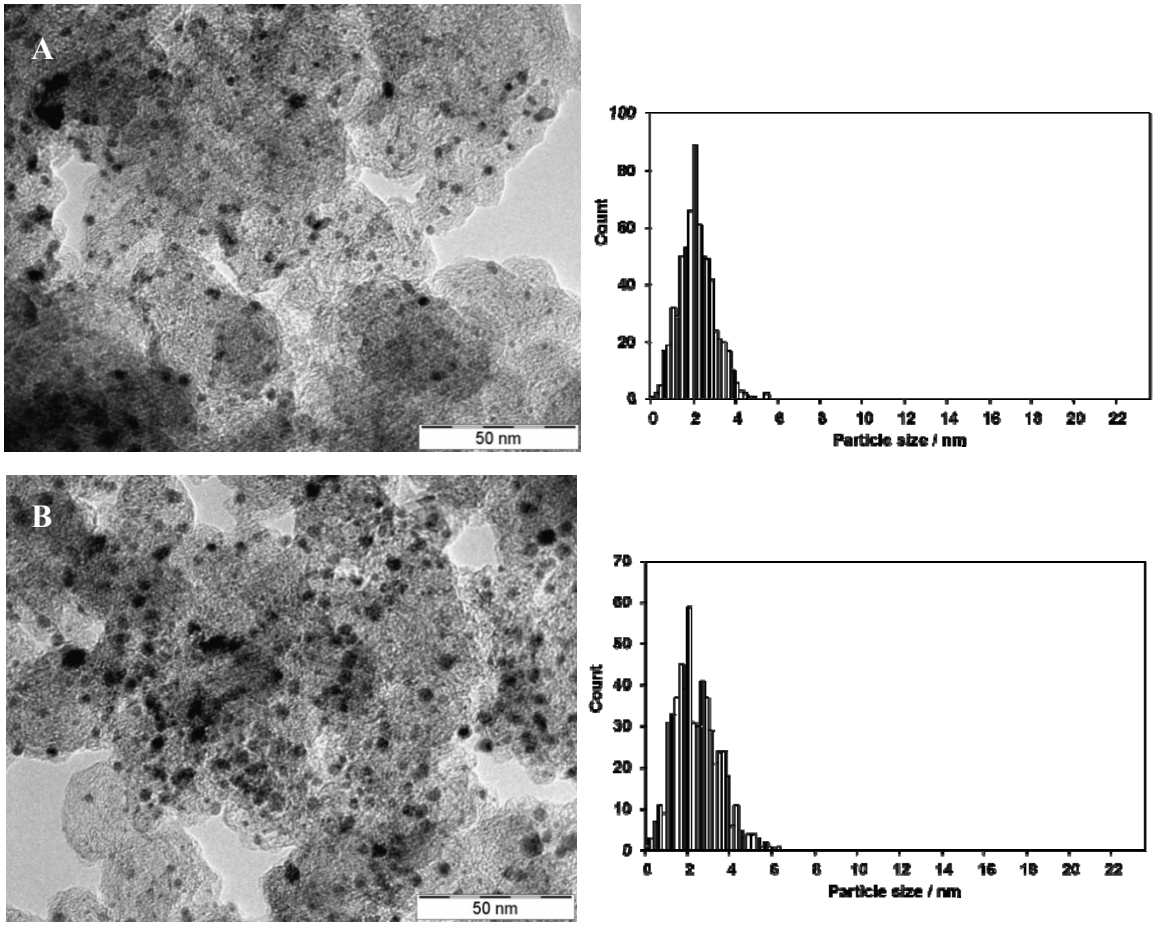

Fig. 3. TEM images and histograms of particle size distribution for (A) the 20Pt/C (H) catalyst and the Sn-20Pt/C-V (H) samples studied after HTT in H_2 at (B) T_{red}= 250 °C and (C) T_{red}= 350 °C.

As shown in Fig. 3 and Table 1 the modification of the 20Pt/C (H) catalyst with tin results in only minor increase of the size of bimetallic particles. Moreover, as shown in Table 1, high dispersion of the Sn-20Pt/C-V (H) catalysts was retained even after HTT in H_2.

SEM and EDX analysis (not shown) of different regions of the samples reveals the coexistence of Sn and Pt particles. No evidence of Sn segregation was evidenced. By focusing the beam in the Sn-modified particles a 25 at.% composition of tin was found, in line with the nominal Pt/Sn atomic ratio of 3.0 used in the preparation and proposed Pt_3Sn crystal phase. Platinum (22.6±1.4 wt.%) and tin (3.8±0.6 wt.%) contents determined by EDX are in good agreement with expected for Pt and Sn values (20 wt.% and 4 wt.%, respectively).

XPS analysis of the Sn-modified home-made 20Pt/C electrocatalyst

The Sn-20Pt/C-V (H) sample was first studied in the *as synthesized* state, without either reductive or oxidative HTT. It is important to note that even in the *as synthesized* state this sample contains some Sn^0 (around 12 %). The Pt/Sn atomic ratio is around 2.2 (see Table S3 in the Supporting material). For this sample the first *in situ* reduction step was carried out at RT. After reductive treatment at RT for 2 h in 300 mbar H_2 the Pt becomes fully metallic and about 60 % of the tin content reduces to Sn^0 (Fig. 4). The Pt/Sn atomic ratio is around 2.5.

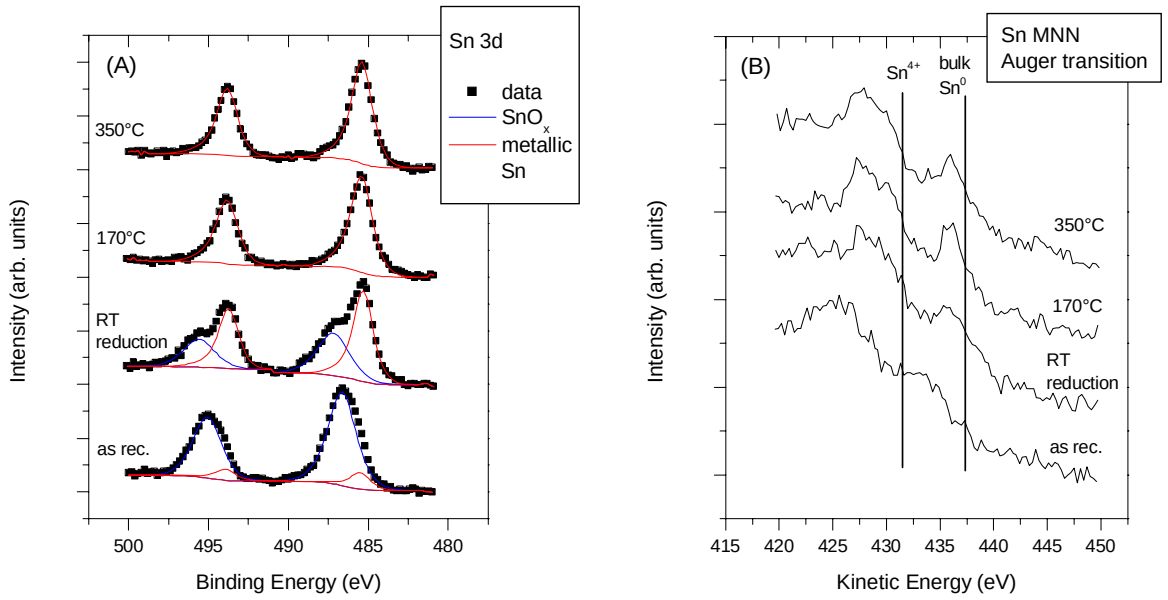

Fig. 4. (A): Sn 3d core level and (B): Sn MNN Auger spectra of the Sn-20Pt/C-V (H) sample in the as synthesized state, after reduction in 300 mbar H_2 for 2 hours at RT, 170 and 350°C. The Sn 3d spectra are corrected for the MgK$\alpha_{3,4}$ satellites.

It may be worth to note that even if RT reduction results in very significant reduction of tin, the Pt/Sn ratio only slightly increases. It means that metallic tin still remains a surface species. Interestingly, the oxidized tin after RT reduction gives rather broad contributions to the Sn 3d spectrum; the oxidized component shifts to a binding energy characteristic for SnO_2, perhaps indicating that the very intimate coupling between tin oxide and Pt became destroyed during reduction. After reduction at 170°C or above, the tin content is fully metallic with the same spectral features as in the case of the Sn-modified Pt/C (Q) catalysts, suggesting alloy formation and the intended Pt/Sn ratio of 3 can be measured.

Ex situ and in situ XRD studies of the Sn-modified home-made 20Pt/C electrocatalysts

Sn-modified 20Pt/C (H) electrocatalysts were studied by XRD techniques after pre-treatment in H_2 at different temperatures (see *ex situ* studies in Table 2).

It is well known that upon formation of the Pt-Sn solid solutions the incorporation of tin into the fcc structure of platinum results in shift of the peaks to lower 2θ values [5,58]. Upon increasing tin content the lattice parameter changes linearly from 3.9231 Å for pure Pt (PDF#04-0802) to 4.0015 Å for Pt_3Sn alloy (PDF#35-1360) [5]. On the other hand, the solubility limit of tin in fcc Pt is still unknown, but is presumed to be around 8-10 at % [59, 60]. In the bulk Pt-Sn phase diagram the composition range between the solubility limit and the 25 at.% Sn content corresponding to the Pt_3Sn intermetallic compound is described as a two-phase region at RT. Accordingly, the lattice constant value of 3.965 Å, found for a

commercial Sn-Pt/C catalyst in Ref. [59] was attributed to a mixture of the saturated $Pt_{90}Sn_{10}$ solid solution (3.934 Å) [61] and stoichiometric Pt_3Sn alloy phase (two-phase model). Nevertheless, it has been proposed that given the near-coincidence of the $Pt_{90}Sn_{10}$ and the Pt_3Sn reflections and the peak broadening due to small particle size, a mixture of these two phases would produce a diffraction pattern very similar to the refined pattern with a nonstoichiometric Pt_3Sn phase.

Table 2. Lattice parameter and particle size calculated for the Sn-20Pt/C-V (H) catalyst reduced at different temperatures.

Samples	Reduction	T_{red}, °C [b)]	Lattice parameter, Å [c)]	Average crystallite size [d)], nm
1	*ex situ* [a)]	250	a: 3.936	7.3
2	*ex situ* [a)]	350	a: 3.936	7.3
3	*in situ*	350	a: 3.955	6.6

[a)] Before XRD measurement the sample was reduced using TPR technique and stored in air;
[b)] Duration of high-temperature reduction: 2 h;
[c)] fcc Pt lattice parameter: a = 3.923 Å, fcc Pt_3Sn lattice parameter: a = 4.0015 Å;
[d)] The Pt particle size of the parent 20Pt/C catalyst: 2.0±1.1 nm.

We reported earlier [34] that upon using CSRs the incorporation of Sn onto 40 wt.% Pt/C (Q) catalyst was achieved satisfactorily yielding a near-stoichiometric fcc Pt_3Sn alloy phase along with a certain amount of the $Pt_{(1-x)}Sn_x$ solid solution; in this system the presence of the ordered Pt_3Sn phase was evidenced by the appearance of weak superlattice reflections. Considering the much smaller particle sizes of the 20 wt.% Pt-containing catalysts of the present work, noting that we were unable to detect the superlattice reflections for these samples and taking into account that at these sizes the bulk phase diagram may not predict adequately the phase distribution, we have decided to use the single-phase model in the evaluation of the XRD data.

As shown in Table 2, the Sn-20Pt/C-V (H) catalyst reduced at 250°C and 350°C (*ex situ* measurement) has a lattice parameter of a= 3.936 Å which is quite close to that of the saturated $Pt_{90}Sn_{10}$ solid solution phase reported by Harris *et al.* [61]. The annealing temperature has no effect on the lattice parameter or the estimated crystallite size. Although the particle sizes determined from the XRD patterns are considerably smaller than in Ref. [34], they are still much larger than those obtained from the TEM data, indicating that the majority of the particles are not accessible for XRD.

Reflections assignable to Sn oxides were not found. However, high sensitivity of the bimetallic Sn-Pt nanoparticles to oxygen is well known [29]. According to our XPS results described above the presence of highly dispersed SnO_x in an "X-ray amorphous" form is expected.

In the next set of experiments the Sn-20Pt/C-V (H) catalyst sample used without any HTT was studied by *in situ* XRD technique. The catalyst was treated in H_2 atmosphere at different temperatures *in situ* and measured in the XRD cell after cooling to RT (details see in Fig. S1 in the Supplementary material and the Experimental part). After *in situ* treatment in H_2 at 350°C for 2 h (see line 3 in Table 2) the refined lattice constant of the Pt-Sn alloy was a= 3.955 Å (between those of Pt_3Sn and Pt) with average particle size of 6.6 nm. Comparison of the lattice constant studied after *ex situ* and *in situ* reduction in the XRD cell at 350°C (see lines 2 and 3 in Table 2) demonstrates that *in situ* treatment results in the Pt-Sn alloy phase

with higher Sn content in the Pt lattice (10 at.% < Sn < 25 at.%), confirming that a certain fraction of tin remained in a non-alloyed, X-ray amorphous form under the *ex situ* conditions.

After *in situ* reduction at 350°C the sample was exposed to air at RT for 24 h, but the difference in the lattice parameter calculated for air-exposed and reduced samples was not observed. However, the formation of amorphous SnO_x phase during the oxidation cannot be ruled out. After RT oxidation only slight increase of the average particle size to 7.6 nm was detected. The observed increase of the particle size is consistent with the suggestion of the appearance of SnO_x forms in the immediate vicinity of the Pt-Sn alloy particles on the platinum-support interface. These results are in good agreement with our *in situ* XPS results demonstrating the reversible interconversion of the Pt-Sn alloy phase into segregated ionic Sn in the presence of O_2. Interestingly, *in situ* diffuse reflectance infrared studies suggested that the small amount of oxygen present under preferential CO oxidation (PROX) conditions is enough for this transformation [56].

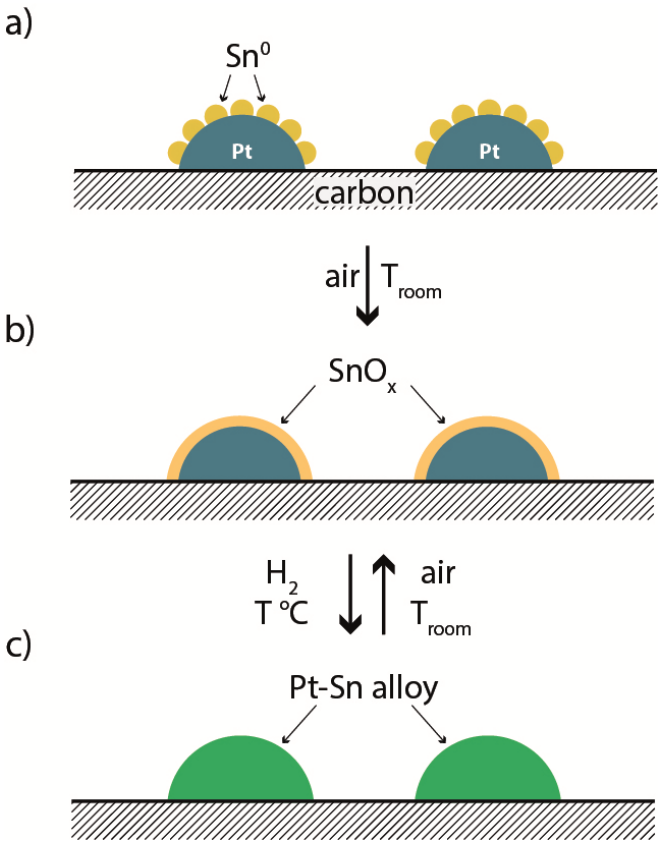

Scheme 1. Proposed model of transformation of various forms of tin in Sn-Pt/C catalysts after different pre-treatments: (a) after tin anchoring reaction at 170°C using P_{H2}= 5 bar; (b) after air exposition at room temperature; (c) after *in situ* reduction of air stored samples.

The schematic view of the proposed transformation of various forms of tin after different pre-treatments based on the *in situ* XPS *in situ* XRD results is shown in Scheme 1.

3.3. Electrochemical characterisation of the Sn-20Pt/C catalysts prepared by CSRs

Fig. 5 compares the CVs and CO-stripping curves recorded on the parent 20Pt/C (Q) and 20Pt/C (H) electrocatalysts with those one obtained on tin-modified samples.

As seen from Fig. 5A and 5C both parent 20Pt/C electrocatalysts show the typical CV of Pt with the classical features of the under-potentially deposited hydrogen adsorption/

desorption between 0.05 < E < 0.40 V. The 20Pt/C (H) electrocatalyst has enlarged double layer region, especially compared to the 20Pt/C (Q) reference catalyst (compare Fig. 5A with Fig. 5C). The observed increase of the double layer signal can be related to large surface area and increased number of the surface functional groups of the Black Pearls 2000 carbon support, compared to Vulcan.

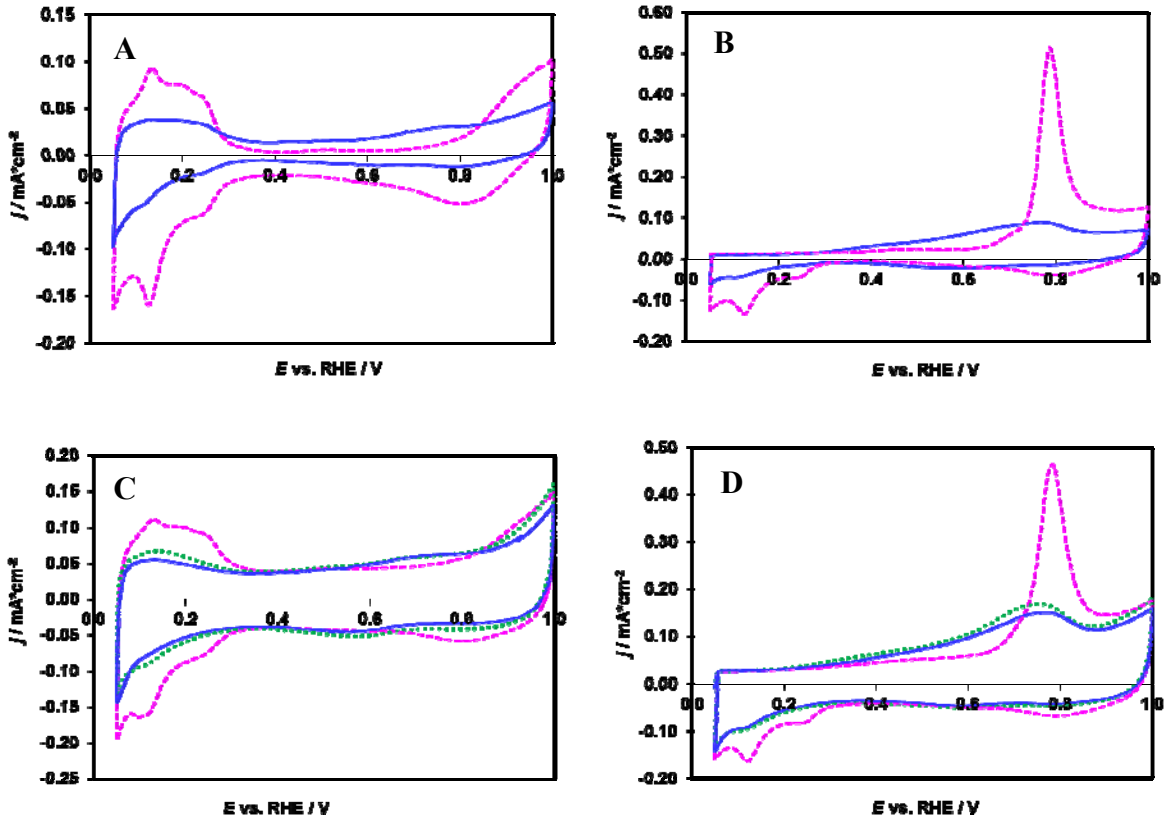

Fig. 5. Influence of tin introduction on the electrochemical performance. Cyclic voltammograms (left) and CO_{ads} stripping voltammograms (right) on the parent 20Pt/C catalysts (dashed pink line) and Sn-modified samples used without TPR (solid blue line). (A, B) the 20Pt/C (Q) and the Sn-20Pt/C-V (Q) samples; (C, D) the 20Pt/C (H) and the Sn-20Pt/C-V (H) samples; for comparison results obtained on the Sn-modified sample reduced at T_{red}= 350 °C (dotted green line) are also included. Recorded in 0.5 M H_2SO_4 at 10 mV s^{-1}. The current was normalized to the geometric surface area.

The CVs of the tin-modified samples showed the rather suppressed hydrogen adsorption/desorption region (see Fig. 5A and 5C). A site-blocking effect caused by tin segregation, probably in a form of thin layer of SnO_x and/or Sn^0 over Pt-Sn alloy phase and/or Pt, can be a reason of the pronounced decrease of H_2 adsorption/desorption. It has been shown by XPS that under oxidative conditions tin in SnO_x form tends to segregate to the surface. The influence of the number of the polarization cycles on the surface composition change of the previously reduced at T_{red}= 350 °C Sn-20Pt/C-V (H) catalyst was demonstrated in Fig. S2 (Supplementary material).

Electrochemically accessible surface area of the platinum can be estimated from these voltammograms using the charge associated with the adsorption/desorption of a hydrogen monolayer for the calculation. In Fig. 6 variation of electrochemically active Pt surface area

on the two parent 20Pt/C catalysts and corresponding Sn-modified samples during the cyclic polarizations are depicted.

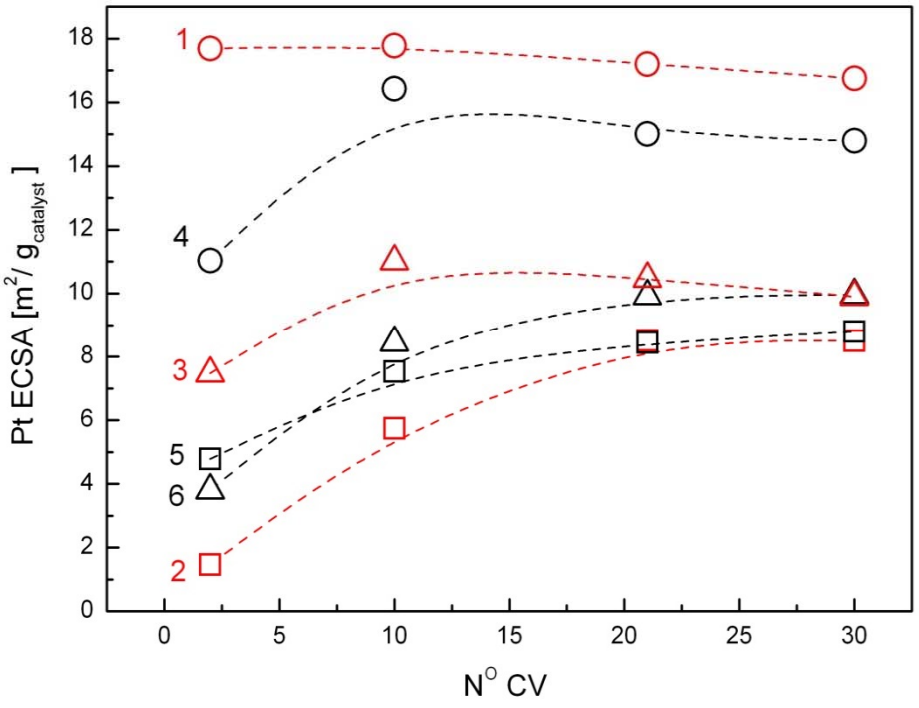

Fig. 6. Surface composition change of catalyst samples during cyclic polarization. Electrochemically active Pt surface area obtained from hydrogen desorption peaks of the cyclic voltammograms as a function of the number of cycles. Curve 1: 20Pt/C (Q); 2: Sn-20Pt/C-V (Q), without TPR; 3: Sn-20Pt/C-V (Q), T_{red}= 350 °C; 4: 20Pt/C (H); 5: Sn-20Pt/C-V (H), without TPR; 6: Sn-20Pt/C-V (H), T_{red}= 350 °C.

The highest $ECSA_H$ values were calculated for two 20Pt/C catalysts. The increase of the $ECSA_H$ value observed between the 2nd and 10th cycles on the 20Pt/C (H) catalyst (see curve 4 in Fig. 6) can be related to the cleaning of the electrode surface from the residual impurities. As shown in Fig. 6 for both parent 20Pt/C catalysts a minor decrease of the $ECSA_H$ values (ca. 6 %) was observed between the 10th and 30th cycles. The behavior of all tin-modified Pt/C catalysts is quite similar: an increase of the $ECSA_H$ values between the 2nd and 10th cycles and relative stability of the surface composition after the 20th cycle is observed. These data indicate the gradual increase of the number of the available Pt sites connected probably to the partial dissolution of the SnO_x species during the first few polarization cycles. The $ECSA_H$ values obtained on the Sn-modified samples pre-treated in H_2 at T_{red}= 350 °C were only slightly higher comparing to those obtained on the Sn-Pt/C samples used without TPR (compare curves 3 and 6 with curves 2 and 5 in Fig. 6).

It can be seen from Fig. 5B and 5D that during the CO stripping cycle the hydrogen features are not observed, reflecting the blocking of the Pt sites due to the presence of adsorbed CO. Once CO_{ad} becomes oxidized (see the positive currents in the voltammograms) the peaks corresponding to the formation of adsorbed hydrogen are clearly visible on the voltammograms, indicating the complete oxidation of CO_{ad}. As shown in Fig. 5B and 5D the onset potential for the oxidation of CO ($E_{CO,onset}$) on both 20Pt/C catalysts was quite similar about 615-625 mV with the peak maximum at 785 mV. The $ECSA_{CO}$ values were calculated

from the charge associated with a CO monolayer adsorbed on the Pt nanoparticles (see Table 1). Our results demonstrate that the commercial and home-made 20Pt/C catalysts have well-dispersed Pt nanoparticles.

A strong promotion of the CO oxidation process is observed on Sn-modified samples when compared to the parent 20Pt/C catalysts. It is necessary to mention that the shape of the CO oxidation peaks presented for the parent and tin-modified catalysts in Figs. 5B and 5D is rather different; CO_{ad} oxidation on Sn-modified Pt/C catalysts is a broad peak from ca. 205 to 850 mV, whereas a rather well defined peak is recorded for the CO_{ad} electrooxidation on both 20Pt/C catalysts. The $E_{CO,onset}$ for the oxidation of CO on Sn-20Pt/C (Q) catalysts was between 215 and 300 mV (see Table 1). In these series of experiments the lowest $E_{CO,onset}$ value (205 mV) was obtained on the Sn-20Pt/C (H) catalyst (see Table 1).

It is well documented that CO oxidation on Sn-modified Pt/C catalysts obey a bifunctional mechanism in which CO is adsorbed on Pt whereas Sn sites nucleate OH_{ad} species at less positive potentials than Pt [62,63]. It should be recalled that CO electrooxidation on Pt-based electrodes takes place in the presence of OH_{ad} species which become nucleated on Pt/C in acid medium at E > 0.6 V but they are available on the surface of Sn-containing electrodes at potentials as low as 200 mV. In particular, by combination of kinetic studies and ambient pressure XPS [48] or diffuse reflectance infrared spectroscopy [56], a bifunctional process was identified as the mechanism behind the enhanced activity of the Pt-Sn bimetallic system in gas phase CO oxidation, during which CO is adsorbed on Pt, while oxygen is activated by Sn^{2+}-like surface species formed under the reaction conditions.

Upon preparation of Pt-Sn catalysts the dilution of the Pt with Sn usually results in some decrease of the ECSA values (see Table 1). As emerges from Table 1 the $ECSA_{CO}$ values calculated for the Sn-modified catalysts were smaller compare to those of the parent 20Pt/C catalysts ($ECSA_{Sn\text{-}20Pt/C}/ECSA_{20Pt/C}$ = 0.75-0.79). Moreover, the $ECSA_{CO}$ values of three Sn-20Pt/C-V (H) samples used after different pre-treatments are noticeably higher comparing to the Sn-20Pt/C (Q) catalysts. Thus the $ECSA_{CO}$ values depends more on the type of the parent catalyst ((Q) or (H)) than on the type of the pre-treatment applied after tin anchoring step I.

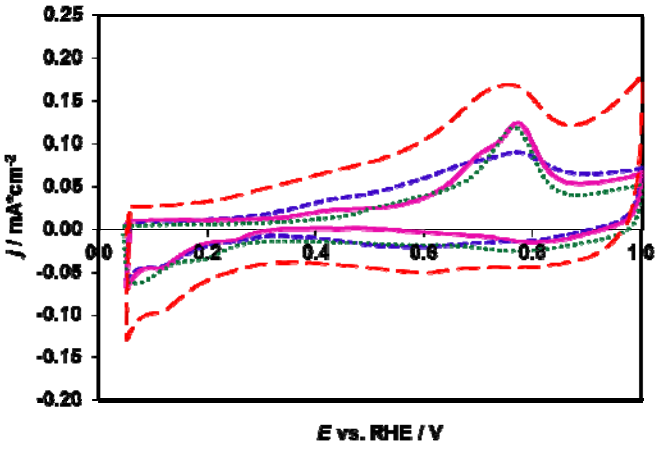

Fig. 7. CO_{ads} stripping voltammograms obtained on Sn-20Pt/C (Q) and (H) electrocatalysts: Sn-20Pt/C-V (H), T_{red}= 350°C (dashed red line); Sn-20Pt/C-III (Q), T_{red}= 250°C (short dashed blue line) and T_{red}= 350°C (solid pink line). For comparison results obtained on the PtRu/C (dotted green line) are included. Recorded in 0.5 M H_2SO_4 at 10 mV s^{-1}. The current was normalized to the geometric surface area.

Fig. 7 compares the CO-stripping curves recorded on Sn-20Pt/C (Q) and (H) electrocatalysts with that one obtained on the state-of-art CO tolerant PtRu/C bimetallic catalyst. In addition, the influence of the T_{red} on the behavior of the Sn-20Pt/C (Q) catalysts in the electrooxidation of CO was also demonstrated. Slight difference observed in the shape of the CO-stripping curves obtained on the Sn-20Pt/C (Q) catalysts (see Fig. 7) can be connected to the different ratio between Pt-Sn alloy phase and the SnO_x surface species obtained after reduction at 250°C and 350°C.

On the PtRu/C catalyst the CO_{ads} is oxidized over a broad potential region starting at potentials of ca. 350 mV with current maximum at 765 mV. It is necessary to mention that the maximum of the main peak observed in this work was shifted to higher potential comparing to the values usually accepted in the literature (650-700 mV [64]). As seen from Fig. 7 significantly better performance for Sn-20Pt/C (H) catalyst was observed. High dispersion of this catalyst retained even after reduction at T_{red}= 350 °C (see Table 1) can be a reason of the increased activity in the electrooxidation of CO.

Catalytic activity of the catalyst samples was tested in the ORR by RDE technique in O_2 saturated 0.5 M H_2SO_4 solution at ambient temperature and pressure. As can be seen from the Koutechky-Levic representation of the data measured at 300 mV applying different rotation speeds (Fig. S3, insert in the Supplementary material) the electrode reaction is under mixed kinetic-diffusion control at this potential. In order to compare the catalysts, mass specific current densities are depicted in Fig. 8. Oxygen reduction currents are normalized to the platinum content of the catalysts in this case. Marked difference has been found between the two groups of parent catalysts considering the onset potential of the ORR. As can be seen in Fig. 8 ***j*** vs. ***E*** curves of 20Pt/C (H) and the two Sn-modified version of this parent catalyst show very similar behavior. Current densities on these samples in the kinetically controlled regime are significantly higher comparing to the Pt/C (Q) and Sn-20Pt/C (Q) samples.

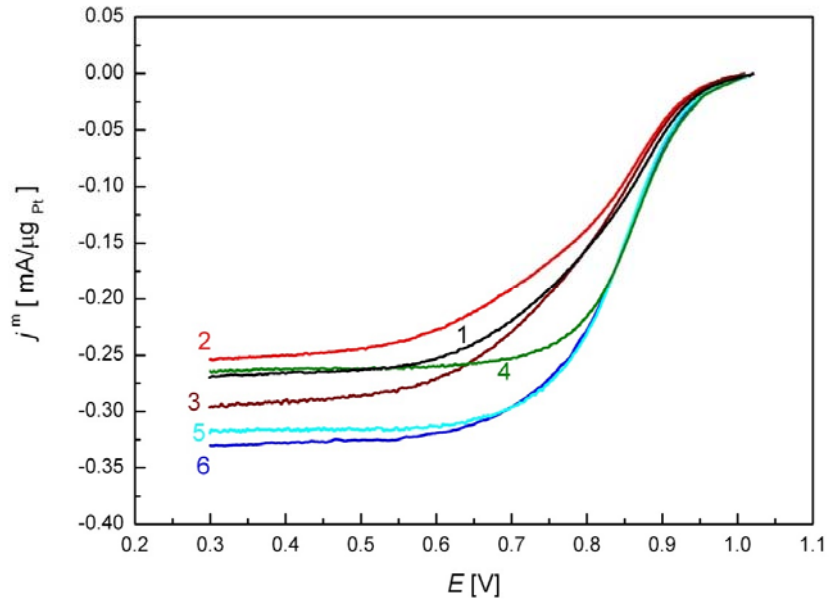

Fig. 8. Oxygen reduction mass specific current densities (negative sweep, 10 mV s^{-1}) measured in O_2 saturated 0.5 mol dm^3 H_2SO_4 on different Pt/C and Sn-Pt/C catalysts at 625 rpm. Curve 1: 20Pt/C (Q); 2: Sn-20Pt/C-V (Q), without TPR; 3: Sn-20Pt/C-V (Q), T_{red}= 350 °C; 4: 20Pt/C (H); 5: Sn-20Pt/C-V (H), without TPR; 6: Sn-20Pt/C-V (H), T_{red}= 350 °C.

Interpretation of the results of RDE measurements on electocatalysts with large surface area and disperse surface have to carried out cautiously [65,66]. Nevertheless, in our case catalyst samples with similar composition and structure were investigated applying the same procedure and electrode preparation technique and the RDE results may contribute to the qualitative description and comparison the catalysts.

As a result of the modification of the 20Pt/C catalysts with tin, electrochemically active Pt surface area of the catalysts decreased. This effect is not surprising and is demonstrated also by Fig. 6. At the same time, the Pt mass specific current densities of the ORR are significantly higher on both reduced at T_{red}= 350 °C Sn-modified catalysts (see curves 3 and 6 in Fig. 8) and even on the Sn-Pt/C (H) catalyst used without TPR (see curve 5 in Fig. 8) compared to the corresponding parent catalysts. On the basis of the RDE measurements it can be concluded that the Sn-Pt/C (H) catalyst reduced at T_{red}= 350 C is the most promising in the ORR among the investigated samples.

The unique increase in the ORR performance of the Pt-Sn(oxidized)/C catalyst in Ref. [7] was ascribed to a promoting effect of SnO_2 nano-islands formed on the surface of Pt_3Sn core nanoparticles. We demonstrated earlier by *in situ* Mössbauer spectroscopy [29] that in the presence of O_2 and H_2 the reversible interconversion of PtSn ↔ Sn^{4+} + Pt can easily proceeded and even after reduction of air stored Sn-Pt supported catalysts at RT the dominating portion of tin (67 %) was readily reconverted to Pt-Sn alloy phase. According to our XPS and XRD results described above the presence of highly dispersed SnO_x thin layer over Pt-Sn alloy phase and/or Pt can also be expected. Therefore, optimal surface composition and high dispersion of the Sn-20Pt/C (H) catalysts results in increased activity in the ORR.

4. Conclusions

Alloy-type Sn-Pt/C electrocatalysts with the desired Pt/Sn= 3.0 ratio have been prepared using commercial 20Pt/C (Q) and home-made 20Pt/C (H) catalysts by means of CSRs. High dispersion of the bimetallic nanoparticles (3.4 nm) for Sn-20Pt/C (H) catalysts was retained even after reduction at T_{red}= 350 °C. However, upon HTT of the Sn-20Pt/C (Q) catalyst in H_2 at 350°C noticeable increase of the particles size up to 5.6 nm was observed. According to *in situ* XPS and *in situ* XRD studies the exclusive incorporation of Sn onto the Pt sites was achieved resulting in exclusive formation of Pt-Sn alloy phase. No evidence of the presence of SnO_2 phase was found by means of the XRD and EDS analysis. Homogeneous distribution of tin in the Pt matrix with mean atomic Pt/Sn ratio of 2.85 was evidenced by EDX analysis. According to *in situ* XPS studies pre-treatment of the air exposed catalyst in H_2 even at 170°C resulted in complete reduction of the ionic tin to Sn^0, suggesting alloy formation. After contact of Sn-Pt/C catalysts with air Sn tends to segregate to the surface, where it oxidizes to a certain extent. Reversible interconversion of PtSn ↔ Sn^{4+} + Pt in the presence of O_2 and H_2 was convincingly demonstrated by *in situ* XPS and *in situ* XRD studies.

The electrocatalytic performance of these novel Sn-20Pt/C electrocatalysts was tested in CO oxidation and ORR. Although initially the majority of Pt sites were blocked by segregated SnO_x, an electrode conditioning consisting of a few polarization cycles removed these species and only minor changes of the catalysts surface composition were observed after 20 cycles. Better performance in the CO electrooxidation for our Sn-Pt/C catalysts compared to the state-of-art CO tolerant PtRu/C benchmark catalyst was demonstrated. Optimal surface composition of the Sn-20Pt/C (H) catalysts results in increased activity in the ORR compared to the Sn-20Pt/C (Q) and both parent 20Pt/C catalysts. On the basis of the RDE measurements it can be concluded that the Sn-Pt/C (H) catalyst reduced at T_{red}= 350 °C is the most promising one in the ORR among the investigated samples.

Acknowledgements

This work was supported by the National Development Agency [grant number KTIA_AIK_12-1-2012-0014]. Financial support by the OTKA-project [grant number K100793 (Zoltán Pászti) and K112034 (István Bakos)] is greatly acknowledged.

References

[1] K.V. Kordesch, G. R. Simader, Chem. Rev. 95 (1995) 191-207.
[2] M.V. Martínez-Huerta, J.L. Rodríguez, N. Tsiouvaras, M.A. Peña, J.L.G. Fierro, E. Pastor, Chem. Mater. 20 (2008) 4249-4259.
[3] M.V. Martínez-Huerta, S. Rojas, J.L. Gómez de la Fuente, P. Terreros, M.A. Peña, J.L.G. Fierro, Appl. Catal. B: Environ. 69 (2006) 75-84.
[4] C.W. Liu, Y.W. Chang, Y.C. Wei, K.W. Wang, Electrochim. Acta 56 (2011) 2574-2581.
[5] S. García-Rodríguez, F. Somodi, I. Borbáth, J.L. Margitfalvi, M.A. Peña, J.L.G. Fierro, S. Rojas, Appl. Catal. B: Environ. 91 (2009) 83-91.
[6] S. García-Rodríguez, M.A. Peña, J.L.G. Fierro, S. Rojas, J. Power Sources 195 (2010) 5564-5572.
[7] G. Samjeské, S. Nagamatsu, S. Takao, K. Nagasawa, Y. Imaizumi, O. Sekizawa, T. Yamamoto, Y. Uemura, T. Uruga, Y. Iwasawa, Phys.Chem. Chem. Phys. 15, (2013) 17208-17218.
[8] M. Arenz, V. Stamenkovic, B.B. Blizanac, K.J. Mayrhofer, N.M. Markovic, P.N. Ross, J. Catal. 232 (2005) 402-410.
[9] E. Antolini, E.R. Gonzalez, Catal. Today, 160 (2011) 28-38.
[10] E. Higuchi, K. Miyata, T. Takase, H. Inoue, J. Power Sources 196 (2011) 1730-1737.
[11] S. García-Rodríguez, S. Rojas, M.A. Peña, J.L.G. Fierro, S. Baranton, J.M. Léger, Appl. Catal. B: Environ. 106 (2011) 520- 528.
[12] L. Li, M. Huang, J. Liu, Y. Guo, J. Power Sources 196 (2011) 1090-1096.
[13] H. Bönnemann, P. Britz, W. Vogel, Langmuir 14 (1998) 6654-6657.
[14] W.J. Zhou, S.Q. Song, W.Z. Li, Z.H. Zhou, G.Q. Sun, Q. Xin, S. Douvartzides, P. Tsiakaras, J. Power Sources 140 (2005) 50-58.
[15] J.H. Kim, S.M. Choi, S.H. Nam, M.H. Seo, S.H. Choi, W.B. Kim, Appl. Catal. B: Environ. 82 (2008) 89-102.
[16] F. Colmati, E. Antolini, E.R. Gonzalez, Electrochim. Acta 50 (2005) 5496-5503.
[17] F.C. Simoes, D.M. dos Anjos, F. Vigier, J.-M. Léger, F. Hahn, C. Coutanceau, E.R. Gonzalez, G. Tremiliosi-Filho, A.R. de Andrade, P. Olivi, K.B. Kokoh, J. Power Sources 167 (2007) 1-10.
[18] F. Somodi, Z. Peng, A.B. Getsoian, A.T. Bell, J. Phys. Chem. C 115 (2011) 19084-19090.
[19] J. Margitfalvi, M. Hegedűs, S. Gőbölös, E. Kern-Tálas, P. Szedlacsek, S. Szabó, F. Nagy, in: Proc. *8th Int. Congress on Catalysis*, Vol. 4, Berlin (West), 2-6 July 1984, pp. 903-912.
[20] J.L. Margitfalvi, I. Borbáth, M. Hegedűs, E. Tfirst, S. Gőbölös, K. Lázár, J. Catal. 196 (2000) 200-204.
[21] J.L. Margitfalvi, S. Gőbölös, in: J.J. Spivey, G.W. Roberts (Eds.), Catalysis, Vol. 17, The Royal Society of Chemistry, Manchester, 2004, pp. 1-104.
[22] J.L. Margitfalvi, I. Borbáth, M. Hegedűs, S. Gőbölös, A. Tompos, F. Lónyi, Stud. Surf. Sci. Catal. 130 (2000) 1025-1030.
[23] J.L. Margitfalvi, I. Borbáth, E. Tfirst, A. Tompos, Catal. Today 43 (1998) 29-49.
[24] J.L. Margitfalvi, I. Borbáth, M. Hegedűs, A. Tompos, Appl. Catal. A: Gen. 229 (2002) 35-49.
[25] Borbáth, I. (2013) *Preparation of bi- and multimetallic supported catalysts by controlled surface reactions*. PhD Dissertation, Budapest University of Technology and Economics, Budapest, Hungary, pp. 124. Retrieved from http://hdl.handle.net/10890/1297

[26] I. Borbáth, F. Somodi, I.M.J. Vilella, S.R. de Miguel, O.A. Scelza, J.L. Margitfalvi, Catal. Commun. 10 (2009) 490-493.
[27] S.A. Bocanegra, S.R. de Miguel, I. Borbáth, J.L. Margitfalvi, O.A. Scelza, J. Mol. Catal. A: Chemical 301 (2009) 52-60.
[28] F. Somodi, I. Borbáth, M. Hegedűs, A. Tompos, I.E. Sajó, K. Lázár, S. Rojas, J.L.G. Fierro, J.L. Margitfalvi, Appl. Surf. Sci. 256 (2009) 726-736.
[29] J.L. Margitfalvi, I. Borbáth, K. Lázár, E. Tfirst, Á. Szegedi, M. Hegedűs, S. Gőbölös, J. Catal. 203 (2001) 94-103.
[30] I.M. Vilella, I. Borbáth, J.L. Margitfalvi, K. Lázár, S.R. de Miguel, O.A. Scelza, Appl. Catal. A: Gen 326 (2007) 37-47.
[31] S. Gőbölös, N. Mahata, I. Borbáth, M. Hegedűs, J.L. Margitfalvi, React. Kinet. Catal. Lett. 74 (2001) 345-352.
[32] W.D. Rhodes, J.L. Margitfalvi, I. Borbáth, K. Lázár, V.I. Kovalchuk, J.L. d`Itri, J. Catal. 230 (2005) 86-97.
[33] J.L. Margitfalvi, S. Gőbölös, E. Tálas, I. Borbáth, Stud. Surf. Sci. Catal. 172 (2007) 177-180.
[34] I. Borbáth, D. Gubán, Z. Pászti, I.E. Sajó, E. Drotár, J.L. Gómez de la Fuente, T. Herranz, S. Rojas, A. Tompos, Top. Catal. 56 (2013) 1033-1046.
[35] T. Herranz, S. García, M.V. Martínez-Huerta, M.A. Peña, J.L.G. Fierro, F. Somodi, I. Borbáth, K. Majrik, A. Tompos, S. Rojas, Int. J. Hydrogen Energy 37 (2012) 7109-7118.
[36] I.C. Hwang, J.H. Ji, P.Kim, J.B. Joo, US Patent 7,838,458 B2 United States of America, november 23, 2010.
[37] N. Fairley, www.casaxps.com, 2006
[38] M. Mohai, Surf. Interface Anal. 36 (2004) 828-832.
[39] M. Mohai, XPS MultiQuant: Multi-model X-ray photoelectron spectroscopy quantification program, Version 3.00.16 (2003) http://www.chemres.hu/aki/XMQpages/XMQhome.htm
[40] C.D. Wagner, A.V. Naumkin, A. Kraut-Vass, J.W. Allison, C.J. Powell, J.R.Jr. Rumble, NIST X-ray Photoelectron Spectroscopy Database, Version 3.4, National Institute of Standards and Technology, Gaithersburg, MD, (http://srdata.nist.gov/xps/), 2003.
[41] J.F. Moulder, W.F. Stickle, P.E. Sobol, K.D. Bomben, Handbook of X-ray Photoelectron Spectroscopy, Perkin-Elmer Corp., Eden Prairie, Minnesota, USA,1992.
[42] H. Schulenburg, J. Durst, E. Müller, A. Wokaun, G.G. Scherer, J. Electroanal. Chem. 642 (2010) 52-60.
[43] J.L. Margitfalvi, I. Borbáth, M. Hegedűs, S. Gőbölös, Appl. Catal. A: Gen. 219 (2001) 171-182.
[44] Z. Paál, A. Wootsch, D. Teschner, K. Lázár, I.E. Sajó, N. Györffy, G. Weinberg, A. Knop-Gericke, R. Schlögl, Appl. Catal. A: Gen. 391 (2011) 377-385.
[45] S.R. de Miguel, M.C. Roman-Martinez, E.L. Jablonski, J.L.G. Fierro, D. Cazorla-Amoros, O.A. Scelza, J. Catal. 184 (1999) 514.
[46] M.C. Román-Martinez, D. Cazorla-Amorós, A. Linares-Solano, C. Salinas-Martinez de Lecea, H. Yamashita, M. Anpo, Carbon 33 (1) (1995) 3-13.
[47] M. Batzill, U. Diebold, Prog. Surf. Sci. 79 (2005) 47-154.
[48] W.D. Michalak, J.M. Krier, S. Alayoglu, J. Shin, K. An, K. Komvopoulos, Z. Liu, G.A. Somorjai, J. Catal. 312 (2014) 17-25.
[49] D.I. Jerdev, B. E. Koel, Surf. Sci. 492 (2001) 106-114.
[50] S. Axnanda, W.P. Zhou, M.G. White, Phys. Chem. Chem. Phys. 14 (2012) 10207-10214.
[51] V. Matolín, I. Matolínová, M. Václavu, I. Khalakhan, M. Vorokhta, R. Fiala, I. Piŝ, Z. Sofer, J. Poltierová-Vejprarová, T. Mori, V. Potin, H. Yoshikawa, S. Ueda, K. Kobayashi, Langmuir 26 (2010) 12824-12831.
[52] L F. Şen, G. Gökağac, J. Phys. Chem. C 111 (2007) 5715-5720.

[53] A. Virnovskaia, S. Jorgensen, J. Hafizovic, O. Prytz, E. Kleimenov, M. Havecker, H. Bluhm, A. Knop-Gericke, R. Schlögl, U. Olsbye, Surf. Sci. 601 (2007) 30-43.
[54] R. Bouwman, P. Biloen, Anal. Chem. 46 (1974) 136-138.
[55] E. Merlen, P. Beccat, J.C. Bertolini, P. Delichere, N. Zanier, B. Didillon, J. Catal. 159 (1996) 178-188.
[56] A. Moscu, L. Veyre, C. Thieuleux, F. Meunier, Y. Scuurman, Catal. Today 258 (2015) 241-246.
[57] A. Moscu, Y. Scuurman, L. Veyre, C. Thieuleux, F. Meunier, Chem. Commun. 50 (2014) 8590-8592.
[58] F. Colmati, E. Antolini, E.R. Gonzalez, J. Solid State Electrochem. 12 (2008) 591-599.
[59] V. Radmilovic, T.J. Richardson, S.J. Chen, P.N. Ross Jr., J. Catal. 232 (2005) 199-209.
[60] T. Biggs, S.S. Taylor, E. van den Lingen, Platinum Metals Rev. 49 (2005) 2-15.
[61] I.R. Harris, M. Norman, A.W. Brayant, J. Less-Common Met. 16 (1968) 427-440.
[62] P. Liu, A. Logadottir, J.K. Norskov, Electrochim. Acta. 48 (2003) 3737-3742.
[63] M.T.M Koper, Surf. Sci. 548 (2004) 1-3.
[64] F. Micoud, F. Maillard, A. Gourgaud, M. Chatenet, Electrochem. Commun. 11 (2009) 651-654.
[65] J. Masa, C. Batchelor-McAuley, W. Schuhmann, R.G. Compton, Nano Research, 7 (2014) 71-78.
[66] C. Batchelor-McAuley, R.G. Compton, J. Phys Chem. C, 118 (2014) 30034-30038.